Evolution of the Near-Field Patterns into the Far-Field in Surface Plasmonic Band Gap Nano-Structures

S. C. Hohng, D. S. Kim and Y. C. Yoon

Department of Physics, Seoul National University, Seoul 151-742

V. Malyarchuk and Ch. Lienau

Max-Born-Institut für Nichtlineare Optik und Kurzzeitspektroskopie, Max-Born-Str. 2a, Berlin D-12489, Germany

J. W. Park, K. H. Yoo and J. Kim

Korea Research Institute of Standards and Science, Daejon 305-600

S. H. Han and Q-Han Park*

Department of Physics, Korea University, Seoul 136-701

We study emission patterns in periodic nano-hole arrays perforated in a metal film. In the near-field region, higher order multiple components of diffraction interfere with each other to generate complicated spatial patterns. These patterns simplify to a sinusoidal one in the intermediate region and become either homogeneous or sinusoidal in the far-field region, depending on whether the excitation wavelength is larger or smaller than the lattice constant. For an incident wavelength much smaller than the lattice constant, complicated patterns can survive into the far-field. Detailed analytic and numerical studies are presented, which show good qualitative agreement with experiment.

I. INTRODUCTION

There has been an upsurge of interest in surface plasmonic band gap structures such as a metal film with periodically perforated nano-hole arrays [1–13], because of its potential use in sub-wavelength pattern formation. Recently, a novel behavior of the nanoscopic emission pattern has been found in this structure [14], showing that the metal surface can shine brighter than the holes. It was also observed that the pattern becomes sinusoidal in the far-field region under certain conditions. A systematic study of these patterns, however, has not yet been made.

In this paper, we focus on how the near-field emission pattern evolves into the far-field region. The initially complicated near-field pattern simplifies as the tip-to-sample distance increases, and in the far field region it becomes either sinusoidal or homogeneous, depending on whether the excitation wavelength is smaller or larger than the lattice constant. This near-to-far-field emission-pattern change is explained through interference between surface plasmon polaritons and diffracted waves. This clearly establishes that survival of the first one or two diffraction orders into the far-field is the key to understanding the pattern evolution.

II. EXPERIMENT

We employ the near-field scanning optical microscope technique [15,16] in probing the transmission geometry. A 200-nm-thick gold film is deposited onto a sapphire substrate. Electron beam lithography and dry-etching processes are used to make a periodic nano-hole array pattern, with a hole diameter of 250 nm and period of 760 nm. A Ti:sapphire laser excites the sample from the sapphire-metal side with near normal incidence and a metal-coated fiber-tip with a sub-100 nm aperture size collects light from the air-metal side.

Figure 1(a) shows a shear force image of our sample. Figures 1(b), (c) and (d) show near-field emission patterns for horizontal, diagonal, and vertical polarizations,
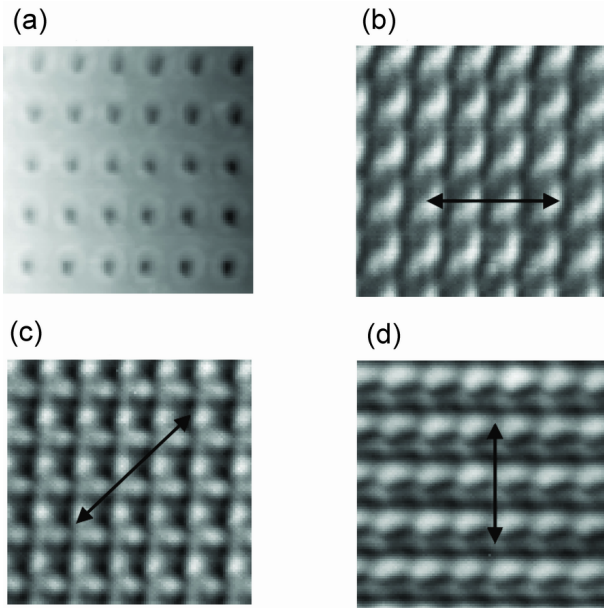
*E-mail: qpark@korea.ac.kr

Fig. 1. (a): Topography of our sample; (b), (c), and (d): Near-field images at different polarizations (arrows). The scanning area is roughly 5 μm $\times$ 5 μm.

Fig. 2. (a) Emission patterns for $\lambda = 820$ nm at $z = 0$, 0.2, and 1.8 μm, from left to right, respectively. (b) Emission patterns for $\lambda = 750$ nm at $z = 0$, 0.55 and 2.9 μm, from left to right, respectively. (c) Cross-sectional scan for the far-right image shown in (a). (d) Cross-sectional scan for the far-right image shown in (b). Dotted lines represent simple sinusoidal fit.

respectively, indicated by the arrows. The excitation wavelength is 780 nm, near the air-metal [1,0] resonance defined as below. These images show stripe-like emission patterns and their orientation runs perpendicular to the incident polarization, reflecting the longitudinal nature of SP excitations. The image repeats itself with the periodicity of lattice, a_0, which strongly suggests that patterns arise through interference between coherently propagating SPs in the $x-y$ plane, each satisfying the periodic boundary condition. The wave vectors of these SP waves are therefore given by $\pm\frac{2\pi}{a_0}(m,n)$ for integers m and n, where m and n can be thought of as the diffraction orders.

Figure 2(a) shows the z-dependence of emission patterns at an excitation wavelength of 820 nm. Between $z = 0$ and $z = 0.2$ μm, the signal intensity decreases while a sinusoidal pattern appears. The sinusoidal pattern further evolves into an essentially homogeneous one with further increasing z. The situation is markedly different when the excitation wavelength becomes smaller than a_0. Shown in Figure 2(b) are the images for an excitation wavelength of 750 nm $< a_0$ in near-field, at $z = 0.55$ and 2.9 μm. Here, the initially complicated pattern becomes spatially sinusoidal with increasing z. In contrast to the longer-wavelength case, the sinusoidal pattern persists up to the far-field region. Shown in Figures 2(c) and (d) are cross-sectional scans of the far-field images shown on the far-right sides of Figures 2(a) and (b), respectively. The cross section at the excitation wavelength 750 nm fits very well with a simple sine function, as shown by the dotted line. We now study the wavelength dependence of the far-field images in more
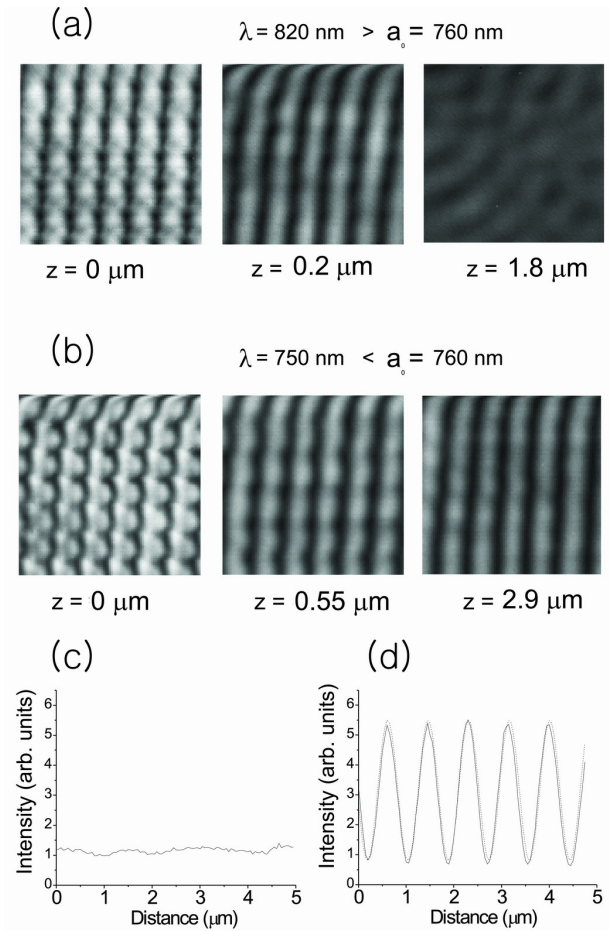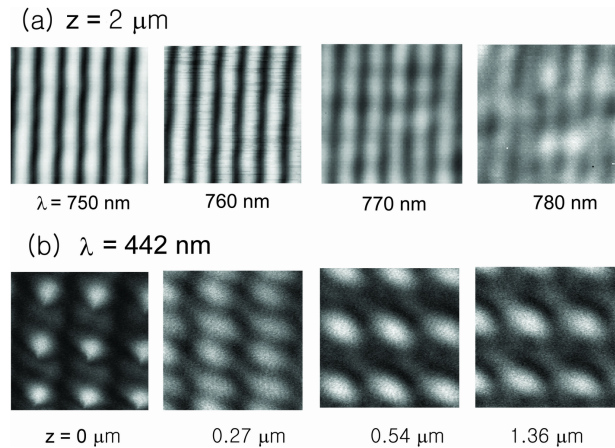

Fig. 3. (a) Emission patterns at a far field region $z = 2$ μm, with varying wavelengths: 750, 760, 770, and 780 nm from left to right, respectively. (b) Emission patterns at the excitation wavelength of 442 nm at different z values as specified. The scanning area is roughly 2 μm $\times$ 2 μm.
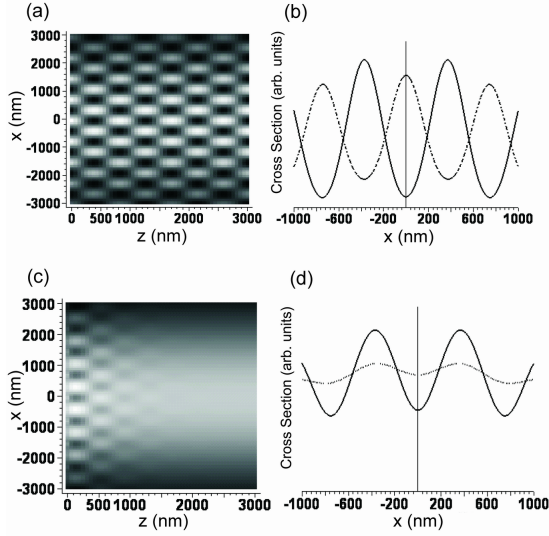
Fig. 4. Emission patterns predicted by diffraction theory. (a) Time-averaged Poynting vector component $\bar{S}_z$ of a Gaussian beam, and (b) cross section through (a) for $\lambda = 740$ nm $< a_0 = 750$ nm, for z = 500 nm (solid line) and 1000 nm (dashed line). (c) and (d) are for the case $\lambda = 780$ nm $> a_0 = 750$ nm. z values for (d) are 200 nm (solid line) and 1000 nm (dashed line).

detail.

Shown in Figure 3(a) are far-field-region images at $z = 2$ μm, at various wavelengths around a_0. At this distance, clear sine waves are seen only up to $\lambda = 760$ nm and the stripe patterns become blurred beyond this point. At an excitation wavelength of 780 nm, the image becomes more or less homogeneous. Clearly, the pattern at the far-field region makes a "transition" around a wavelength equaling a_0. When the wavelength becomes shorter, the pattern becomes more localized and preserved into the far-field region, as shown in Figure 3(b). In the following, we show that a linear superposition of SP waves explains all the essential features of the observed patterns.

III. ANALYTIC AND NUMERICAL RESULTS

To understand the experimental results, we first observe that radiation patterns in the far-field region appear as stripes perpendicular to the polarization direction, irrespective of the details of hole geometry. This suggests that the experiment can be described effectively by diffraction at nano-slits instead of a rigorous diffraction analysis at nano-holes. Thus, in the following analysis, we assume that the system is symmetric along the slit direction, which we choose to be the y-direction. The electric field lies in the xz-plane. In the experimental measurement, we are concerned with the z-component of the Poynting vector, $S_z = E_x H_y$. The electric field
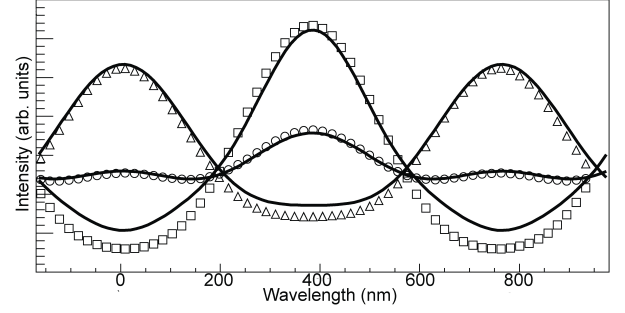

Fig. 5. Emission patterns calculated by the FDTD method. Results are in arbitrary units for $\lambda = 750$ nm $< a_0 = 760$ nm, for z = 500 (box), 1000 (triangle) and 1500 nm (circle). Solid lines are results predicted by diffraction theory with $A_0 = 1.31 \times 10^{-2}$, $A_1 = 0.58 \times 10^{-2}$, and $A_2 = -0.066 \times 10^{-2}$.

component E_x is given by

$$
\begin{aligned}
E_x &= \sum_{n=0}^{r-1} 2A_n \cos(2\pi nx/a) \\
&\times (\cos k_n z \cos wt + \sin k_n z \sin wt) \\
&+ \sum_{n=r}^{\infty} 2A_n \exp(-h_n z) \cos(2\pi nx/a) \cos wt, \quad (1)
\end{aligned}
$$

where coefficients A_n specify relative excitation strengths of each mode and the integer r denotes the number of radiating modes determined such that the n-th order momenta k_n and h_n defined by

$$
\begin{aligned}
k_n &\equiv \sqrt{(2\pi/\lambda)^2 - (2\pi n/a)^2}, \; n < r, \\
h_n &\equiv \sqrt{-(2\pi/\lambda)^2 + (2\pi n/a)^2}, \; n \geq r \quad (2)
\end{aligned}
$$

are all real. The nonvanishing electric field component E_z and the magnetic field component H_y can be obtained directly by integrating Maxwell's equations:

$$
\begin{aligned}
\nabla \cdot \vec{E} &= \partial_x E_x + \partial_z E_z = 0, \\
-\frac{1}{c}\frac{\partial H_y}{\partial t} &= \partial_z E_x - \partial_x E_z. \quad (3)
\end{aligned}
$$

Coefficients A_n can be determined by means of a modal formalism approximation which uses the surface impedance as boundary conditions on the metal surface [17]. Detailed expression of A_n does not concern us here and we simply refer the reader to Ref. [17], from which A_n can be readily obtained with a minor modification.

Consider first the case where the excitation wavelength is slightly shorter than the lattice constant, $\lambda < a_0$, so that $r = 2$. That is, only the homogeneous ($n = 0$) and the first order diffraction mode ($n = 1$) are radiating. Higher order modes ($n \geq 2$) are all evanescent. In the far field region where only the radiating mode survives, the time average of S_z can be readily computed to give

$$
\begin{aligned}
c\bar{S}_z \;=\; & 2A_0^2 + 2A_0A_1\cos(2\pi x/a)\cos[(k_0-k_1)z](1+\frac{k_0}{k_1}) + 2A_1^2\cos^2(2\pi x/a)\frac{k_0}{k_1} \\
& + \; 2A_0A_2e^{-h_2z}\cos(4\pi x/a)\left[\cos(k_0z)-\frac{k_0}{h_2}\sin(k_0z)\right] \\
& + \; 2A_1A_2e^{-h_2z}\cos(2\pi x/a)\cos(4\pi x/a)\frac{k_0}{k_1}\left[\cos(k_1z)-\frac{k_1}{h_2}\sin(k_1z)\right],
\end{aligned}
\tag{4}
$$

where we suppressed contributions from higher-order terms. More realistically, we could include a Gaussian modulation factor to E_x along the x-direction in order to simulate the Gaussian beam and derive the time average of S_z by following the same procedure as above. Figure 4 displays analytic results computed in this way. In all cases, the lattice constant was 750 nm and the Gaussian beam width was assumed to be 8 μm.

Shown in Figure 4(a) and (b) are the time average of S_z and its transversal cross sections at two different z values for $\lambda < a_0$. The zeroth- and the first-order modes persist into the far-field region and their mutual interference generates well-defined spatially sinusoidal waves. In particular, Eq. (4) shows that the period of patterns in the propagation direction is given by

$$
\lambda \left[1 - \left(1 - \frac{\lambda^2}{a^2}\right)^{1/2}\right]^{-1},
\tag{5}
$$

which is bigger than the wavelength λ. It also shows that the relative contribution of the first diffraction order, $n = 1$, is enhanced by $\left(1 - \lambda^2/a^2\right)^{-1/2}$, increasing the modulation depth of the spatial sine wave.

When the excitation wavelength is longer than the lattice constant, $\lambda > a_0$, only the homogeneous ($n = 0$) mode radiates. All other diffraction modes are evanescent and decay exponentially. Figures 4(c) and (d) show the time average of S_z and the cross sections in this case, where the interference between the homogeneous and the decaying diffraction modes can be explicitly observed. These analytical results agree well with a direct numerical result by using the 2-dimensional FDTD (Finite-Difference Time-Domain) method. In performing the FDTD calculation, we assumed a dielectric constant of the Drude type in the metal [18] and measured the time average of S_z at various locations. Figure 5 compares numerical results with the results obtained from Eq. (4), which shows a good agreement particularly in the far field region ($z = 1500$ nm). The agreement is relatively poor in the near field case ($z = 500$ nm) due to the neglect of higher diffraction orders.

For wavelengths much shorter than a_0, which is the case for Figure 3(b), more modes can be radiating and therefore more complicated patterns are preserved. It should be noted that for the excitation wavelength of 442 nm, r should be larger than 2, since the SP group velocity decreases with increasing photon energy [19]. Then,

even in the far-field region, a variety of wave-vector components can participate in the pattern generation. This qualitatively explains why the initial pattern evolves neither to a homogeneous nor to a sinusoidal pattern as z increases, but remains relatively similar to the near-field pattern.

IV. CONCLUSION

In conclusion, we have studied the near-field to far-field evolution of the emission patterns of a plasmonic band gap structure. We can generate tunable, spatially symmetric far-field emission patterns that may be homogeneous or sinusoidal or, in general, polarization- and wavelength-tunable interferences of a few radiating diffraction orders.

ACKNOWLEDGMENTS

REFERENCES

[1] T. W. Ebbesen, H. J. Lezec, H. F. Ghaemi, T. Thio and P. A. Wolff, Nature **391**, 667 (1998).
[2] T. J. Kim, T. Thio, T. W. Ebbesen, D. E. Grupp and H. J. Lezec, Opt. Lett. **24**, 256 (1999).
[3] T. Thio, H. F. Ghaemi, H. J. Lezec, P. A. Wolff and T. W. Ebbesen, J. Opt. Soc. Am. B **16**, 1743 (1999).
[4] D. E. Grupp, H. J. Lezec, K. M. Pellerin, T. W. Ebbesen and T. Thio, Appl. Phys. Lett. **77**, 1569 (2000).
[5] U. Schröter and D. Heitmann, Phys. Rev. B **58**, 15419 (1998).
[6] J. A. Porto, F. J. Garcia-Vidal and J. B. Pendry, Phys. Rev. Lett. **83**, 2845 (1999).
[7] W.-C. Tan, T. W. Preist and J. R. Sambles, Phys. Rev. B **62**, 11134 (2000).
[8] L. Salomon, F. Grillot, A. V. Zayats and F. de Fornel, Phys. Rev. Lett. **86**, 1110 (2001).

[9] L. Martin-Moreno, F. J. Garcia-Vidal, H. J. Lezec, K. M. Pellerin, T. Thio, J. B. Pendry and T. W. Ebbesen, Phys. Rev. Lett. **86**, 1114 (2001).

[10] Y. Takakura, Phys. Rev. Lett. **86**, 5601 (2001).

[11] S. J. McNab, R. J. Blaikie and M. M. Alkaisi, J. Vac. Sci. Technol. B **18**, 2900 (2000).

[12] M. M. Alkaisi, R, J. Blaikie, S. J. McNab, R. Cheung and D. R. S. Cumming, Appl. Phys. Lett. **75**, 3560 (1999).

[13] Q. Cao and P. Lalanne, Phys. Rev. Lett. **88**, 057403 (2002).

[14] S. C. Hohng, Y. C. Yoon, D. S. Kim, V. Malyarchuk, R. Muller, Ch. Lienau, J. W. Park, K. H. Yoo, J. Kim, H. Y. Ryu and Q. H. Park, Appl. Phys. Lett. **82**, 3239 (2002).

[15] D. W. Pohl, W. Denk and W. Lanz, Appl. Phys. Lett. **44**, 651 (1984).

[16] E. Betzig, J. K. Trautman, T. D. Harris, J. S. Weiner and R. L. Kostelak, Science **251**, 1468 (1991).

[17] H. Lochbihler, Phys. Rev. B **50**, 4795 (1994).

[18] K. Sakoda, N. Kawai, T. Ito, A. Chutinan, S. Noda, T. Mitsuyu and K. Hirano, Phys. Rev. B **64**, 045116 (2001).

[19] H. Raether, *Surface Plasmons on Smooth and Rough Surfaces and on Gratings* (Springer, Berlin, 1988).